

Spin physics at COMPASS: present and future

G. K. MALLOT

*European Organization for Nuclear Research, CERN
1211 Genève 23
Switzerland*

Summary. — The lecture discusses the COMPASS experiment at CERN performing deep inelastic scattering of polarised muons off polarised targets. The main results from the measurements performed since 2002 with longitudinal and transverse target polarisation are presented. The second part of the lecture discusses the plans and preparations for future measurements related to generalised parton distributions and transverse-momentum-dependent distribution functions. These experiments comprise deeply virtual Compton scattering as well as hard exclusive meson production in muon scattering off a liquid hydrogen target on the one hand and Drell–Yan dimuon production using a negative pion beam and a transversely polarised proton target on the other hand. During the GPD muon experiment, precise data will also be taken on hadron production and transverse-momentum-dependent distributions with the unpolarised proton target.

1. – Introduction

Partons were discovered at SLAC in the 1960's when scattering electrons from nuclei at large momentum transfers Q^2 . The observed Q^2 independence of the hadronic part of the cross-section, the structure functions, revealed point-like constituents in the nucleon. Later these partons were identified with the quarks. The eventually observed weak Q^2

	1970	1980	1990	2000
SLAC		E80		E130
			E142/3 E154/5	
CERN			EMC	SMC
				COMPASS I
DESY			HERMES	
JLab				CLAS/HALL-A
RHIC				Phenix/Star

Fig. 1. – Laboratories and experiments studying spin-dependent structure functions of the nucleon.

dependence of the structure functions could be attributed to the splitting of partons, i.e. quarks and gluons, into partons with a smaller momentum fractions in the infinite momentum frame. At the electron-proton collider HERA at DESY the spin-independent quark and gluon distributions were then finally studied with high precision at very large momentum transfer and down to tiny momentum fractions.

A detailed understanding of the nucleon structure must include spin degrees of freedom and ultimately should explain the nucleon spin of $1/2\hbar$. The first attempt to study the spin-dependent structure functions of the nucleon was made at SLAC followed by the EMC experiment at CERN which showed in 1988 that the quark spins contribute little to the nucleon spin. Triggered by this entirely unexpected result, experiments were subsequently launched at CERN (SMC, COMPASS), SLAC (E142/3, E154/5), DESY (HERMES), and RHIC (STAR, PHENIX) in order to check the SMC result and to measure the structure functions of the neutron/deuteron (fig. 1). The results confirmed the findings by EMC for the proton and revealed a similar situation for the neutron. The effects in the proton and neutron cancel in the fundamental Bjorken sum rule, which links the difference of proton and neutron spin-dependent structure functions to the neutron weak decay constant g_V/g_A .

After the small quark spin contribution to the nucleon spin was established unambiguously, the focus turned on the gluon polarisation. In this situation the COMPASS Collaboration was founded in 1996 and the experiment was approved in 1998 with first data taking in 2002. Contrary to the previous SMC experiment, which focused on inclusive scattering, the COMPASS spectrometer is optimised for large hadron acceptance and hadron identification in semi-inclusive deep inelastic scattering (SIDIS). The primary goals of the first phase of COMPASS until 2012 are measurements of the spin-dependent quark distributions or the light flavours g_1^q (or Δq), the size of the gluon polarisation g_1^g

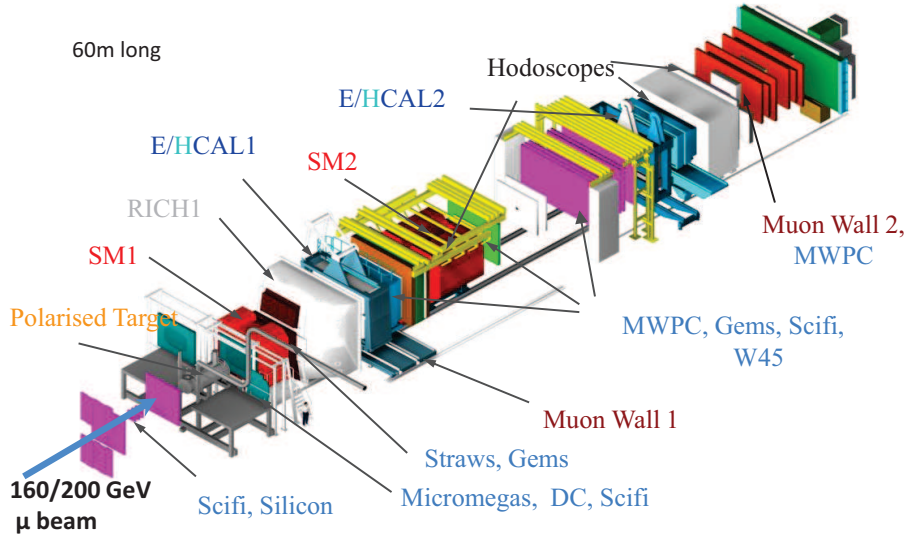


Fig. 2. – The COMPASS spectrometer, for a description see text.

or (or Δg), and the Collins and Sivers asymmetries and thus transversity h_1 (or $\Delta_T q$) and the Sivers function f_{1T}^\perp . After a description of the COMPASS spectrometer in section 2, these results will be discussed in sections 3 and 4. Another large part of the programme not presented here concerns hadron spectroscopy and tests of chiral perturbation theory including a dedicated measurement of the pion polarisability.

Section 5 covers the approved COMPASS plans for the nearer future 2014–2016/7. Here the Collaboration will focus on generalised parton distribution functions (GPDs) and transverse-momentum-dependent (TMD) parton distribution functions. The former will be studied in deeply virtual Compton scattering off a liquid hydrogen target and the latter by Drell-Yan (DY) reactions of a negative pion beam impinging on a transversely polarised proton target.

2. – The COMPASS experiment at CERN

A schematic view of the COMPASS spectrometer [1] is presented in fig. 2. A polarised muon beam of energy 160–200 GeV and with a polarisation of about 80% impinges from the left on a solid-state polarised target consisting of two or three cells with proton or deuteron target material polarised in opposite directions. The usable beam intensity is typically $2 \times 10^7/s$ during a 9.6 s long spill. The repetition rate varies and was typically about 1/40 s. The momentum of each beam particle is measured in the beam momentum station. Downstream of the target, the scattered muon and produced hadrons are detected in a two-stage magnetic spectrometer with the two dipole magnets, SM1 and SM2.

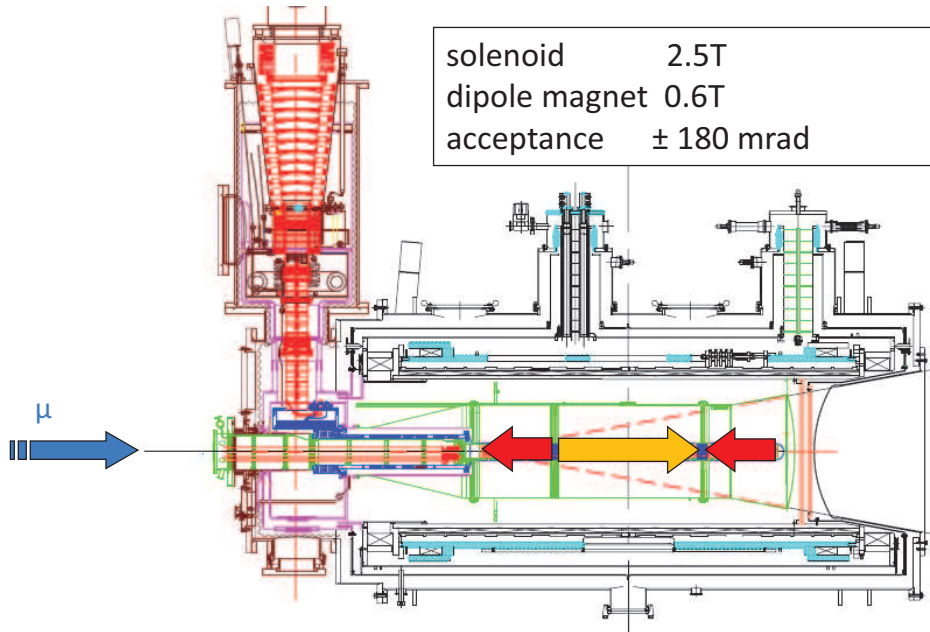


Fig. 3. – The COMPASS polarised target system.

Charged particles are tracked in the beam regions by scintillating fibre stations (Scifi) and by silicon detectors. In the inner region close to the beam, gaseous detectors of the micromegas and GEM types are deployed. Both are based on very small multiplication gaps with high field strength where the electron avalanche develops. The positive charges produced in these gaps can be evacuated rapidly which leads to high rate capabilities. The backbone of tracking in the intermediate region are multiwire proportional chambers (MWPC). Finally, the large area tracking away from the beam region is covered by drift chambers (DC, W45) and drift tubes (Straws, Muon Wall 1 and 2, Rich Wall (not shown)).

The velocity of charged particles is measured in a ring-imaging Cherenkov detector (RICH), which can separate pions and kaons from 9 GeV up to 50 GeV. The Cherenkov photons are emitted along the 3 m long path in the radiator volume filled with the heavy C_4F_{10} gas. In total 116 mirrors reflect light from ultraviolet to visible to the photon detectors with about 80k analog read-out channels. The inner quarter of the photon detector is made by multianode-photomultiplier tubes, while the outer part relies on MWPCs with a photosensitive CsI cathode.

The energy of charged particles is measured in sampling hadron calorimeters (HCAL 1 and 2), while neutral particles, in particular high-energy photons, are detected in electromagnetic calorimeters (ECAL1 and 2). They comprise lead glass modules as well as scintillator/lead ‘shashlik’ modules in the inner high-radiation region.

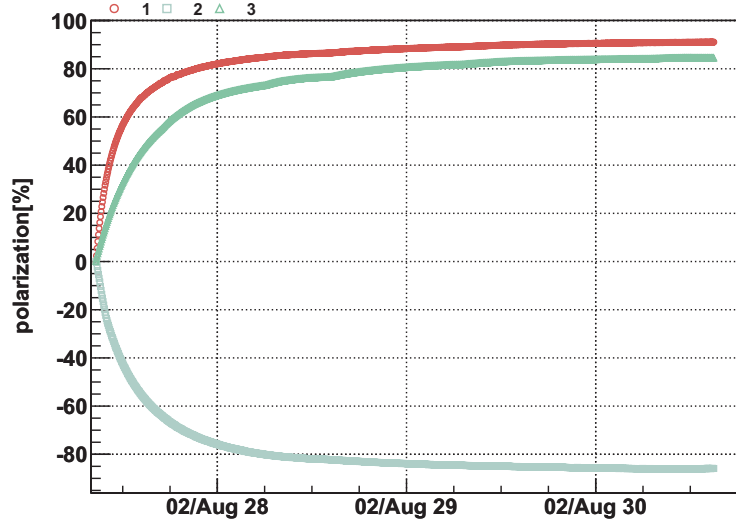


Fig. 4. – Polarisation build-up for the 3-cell ammonia target in 2007 for the outer cells (upper curves) and central cell (lower curve).

Event recording is triggered by the scattered muon, which is ‘identified’ by its ability to traverse thick hadron absorbers, located just upstream of the Muon Wall detectors. The event selection is based on various systems of scintillator hodoscopes and logic modules applying selections criteria like target pointing and energy loss in the scattering. The patterns causing a trigger were optimised by Monte Carlo simulations. The spectrometer has about 250k read-out channels, which can be recorded with a frequency of 20 kHz for an event length in the order of 40 kByte.

The heart of the experiment is the polarised target system (fig. 3). While the muon beam comes naturally polarised due to the parity violation in the decay of the parent pions, polarising protons and deuterons is very difficult. Gas targets can not be used with the muon beam due to the low beam intensity compared to electron beams. An advantage of muon beams is the high muon energy, which presently can not be reached by electron beams. The polarised target system comprises a 2.5 T solenoid magnet, a 0.6 T dipole magnet, a $^3\text{He}/^4\text{He}$ dilution refrigerator, a 70 GHz microwave system and an NMR system to measure the target polarisation. The target material is cooled down to about 60 mK in frozen spin mode. In the presence of the 2.5 T field all free electrons are polarised. Their polarisation is transferred to the protons and deuterons by microwave irradiation. This process of dynamic nuclear polarisation can only be used with few materials. In COMPASS irradiated ammonia (NH_3) and lithium-6 deuteride (^6LiD) were selected as proton and deuteron targets, respectively. Lithium-6 is very close to a system of a free deuteron and a helium-4 core and has essentially the same magnetic moment as the deuteron. Thus ^6LiD

TABLE I. – *Data taking of COMPASS.*

period	beam	target	polarisation
2002–2004	muon	'deuteron'	long. & transv.
2005	CERN accelerator shutdown		
2006	muon	'deuteron'	long.
2007	muon	'proton'	long. & transv.
2008–2009	hadron	hydrogen, nuclear	–
2010	muon	'proton'	transv.
2011	muon	'proton'	long.
2012	hadron	Ni	–
2013	CERN accelerator shutdown		

corresponds to two deuterons plus a helium nucleus. Typically, polarisations of 85% for protons and 50% for deuterons were reached (fig. 4). A key feature of COMPASS is that both target polarisations are present simultaneously in separate target cells along the beam, e.g. ' \rightarrow, \leftarrow ' for the two-cell configuration till 2004 and ' $\rightarrow, \leftarrow, \rightarrow$ ' for the three-cell configuration from 2006 onwards. Thus in an asymmetry measurement most systematic uncertainties cancel. Using the dipole and solenoid magnet, the magnetic field can be rotated from e.g. pointing downstream to transverse to upstream. The spin follows the magnetic field adiabatically and thus the spin orientations can be changed within 30 min. Such a field rotation is performed typically once per day for the longitudinal polarisation in order to cancel potentially remaining systematic effects. The field can also be kept transverse for measurements with transverse target polarisation. Here the polarisation is inverted by repolarising typically once per week. In the shutdown year 2005 the superconducting target magnet was replaced by a new one, increasing the angular acceptance from ± 70 mrad to ± 180 mrad.

The experiment takes data since 2002 (Table I). The years 2008–2009 were dedicated to the hadron spectroscopy programme of COMPASS with pion, kaon and proton beams. In 2012 the pion polarisability will be measured using a negative pion beam and a thin nickel target. Later in this year a pilot run for deeply virtual Compton scattering and hard exclusive meson production will take place.

3. – Longitudinal spin structure results

3'1. Quarks. – Studies of the longitudinal spin structure of the nucleon in deep inelastic scattering (DIS) proceed via the determination of cross-section asymmetries. Such measurements require a longitudinal polarisation of both the incoming lepton and the target nucleon. The process is sketched in fig. 5. Measured is the event number asymmetry $A_{exp} = (N^{\vec{z}} - N^{\vec{\lambda}})/(N^{\vec{z}} + N^{\vec{\lambda}})$, where the single and double arrows indicate the beam and target polarisations, respectively. As in COMPASS the two target polarisations are measured simultaneously with the same beam, flux and acceptance cancel to first

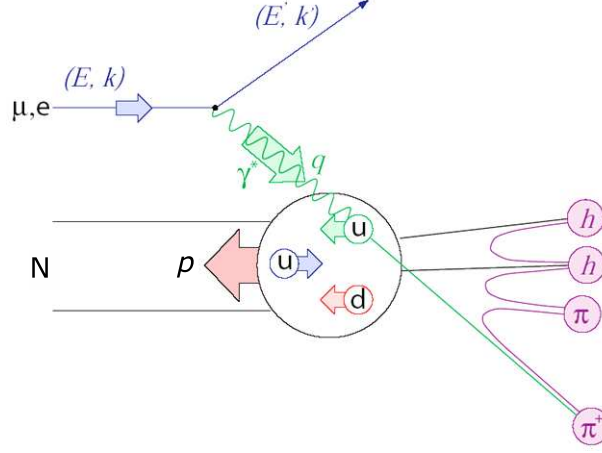


Fig. 5. – Sketch of semi-inclusive deep inelastic scattering off a nucleon.

order and A_{exp} is proportional to the virtual-photon nucleon cross-section asymmetry

$$(1) \quad A_1 = \frac{1}{f P_\mu P_T D} A_{exp}.$$

Here P_μ and P_T denote the beam and target polarisations, and D is the depolarisation factor, which describes the polarisation transfer from the lepton to the virtual photon. The ratio of the spin-averaged cross-section due to all polarisable nucleons in the target to that of all nucleons in the target is the dilution factor f . The factors D and f lie between 0 and 1. For the targets used, the dilution factor varies from about 0.15 for NH_3 to 0.4 for ${}^6\text{LiD}$.

In terms of the parton distribution functions (PDF) g_1 and f_1 , the asymmetry A_1 is given in leading order (LO) by

$$(2) \quad A_1 = \frac{\sum_q e_q^2 g_1(x, Q^2)}{\sum_q e_q^2 f_1(x, Q^2)}$$

and for semi-inclusive DIS by

$$(3) \quad A_1^h = \frac{\sum_q e_q^2 g_1(x, Q^2) D_{1q}^h(z, Q^2)}{\sum_q e_q^2 f_1(x, Q^2) D_{1q}^h(z, Q^2)}.$$

Here, $Q^2 = -(k - k')^2$ is the negative square of the 4-momentum transfer and $x = Q^2/(2Pq)$ is the Bjorken scaling variable, indicating the momentum fraction of the nucleon carried by the struck quark in the infinite momentum frame. For SIDIS, the fragmentation functions (FF) D_{1q}^h describe the fragmentation of a quark q into a hadron h .

In addition to Q^2 they depend on the the laboratory energy fraction $z = E_h/\nu$, which the observed hadron carries with respect to the total energy transfer ν from the lepton to the nucleon.

The proton [2] and deuteron [3] asymmetries measured by COMPASS are presented as a function of x in figs. 6 and 7, respectively. Only asymmetries for $Q^2 > 1 \text{ GeV}^2$ are shown. The inclusive asymmetries, i.e. not requiring an additional hadron, are shown on the left, followed by the asymmetries for identified pions and kaons. Note that kaon measurements for the proton only exist from COMPASS. The spin-dependent structure functions g_1^p and g_1^d corresponding to the inclusive asymmetries are shown in figs. 8 and 9.

The fundamental Bjorken sum rule links the first moment Γ_1^{NS} of the non-singlet structure function $g_1^{NS}(x, Q^2) = g_1^p(x, Q^2) - g_1^n(x, Q^2)$ to the ratio of the axial to vector coupling constants in the neutron beta decay g_A and g_V

$$(4) \quad \Gamma_1^{NS}(Q^2) = \frac{1}{6} \left| \frac{g_A}{g_V} \right| C_1^{NS}(Q^2).$$

The neutron structure function g_1^n can be obtained from the proton and deuteron structure functions and the coefficient function C_1^{NS} describing higher order corrections is known from theory to third order in α_s .

From the COMPASS proton and deuteron data this sum rule can be tested very accurately. We obtain $|g_A/g_V| = 1.28 \pm 0.07$ (stat.) ± 0.10 (syst.) compared to 1.2694 ± 0.0028 from neutron β decay. The values are in excellent agreement and thus the Bjorken sum rule is confirmed at the 10% level (fig. 10).

From the semi-inclusive asymmetries, the quark distributions can be determined for the various flavours starting from eq. 3. The information on the initially struck quark is partly preserved in the fragmentation process and parametrised by the FFs. An up quark prefers to fragment into a positive pion while a down quark prefers fragmenting into a negative pion. Using isospin symmetry and the rather well known fragmentation functions of up and down quarks as well as the poorly known fragmentation functions of strange quarks, one can build a system of equations containing the measured inclusive asymmetries, the asymmetries for identified hadrons as well as the wanted PDFs of the individual flavours. A fit with six flavours (u, d, s and antiquarks) did not show any significant difference for strange quarks and antiquarks. Therefore a five flavour fit with $\Delta s = \Delta \bar{s}$ was used for the result shown in fig. 11 as a function of x [2]. The up quark polarisation is strongly positive at $x > 0.1$, i.e. the spins of the up (down) quark point predominantly in the same direction as that of the proton (neutron). The down quark polarisation is negative and the combined strange and antistrange quark polarisation is slightly negative. The latter comes from the region $x < 2 \times 10^{-2}$, while for larger x the distribution Δs rather vanishes.

Of particular interest are the first moments of the spin-dependent quark distributions $\Delta q = \int \Delta q(x) dx$. They are given for $Q^2 = 3 \text{ GeV}^2$ in table II. The regions unmeasured by COMPASS, $0 < x < 0.004$ and $0.7 < x$, were extrapolated using the PDFs from the DSSV fit [5]. The range $0.3 < x < 0.7$ was taken from the inclusive data assuming that

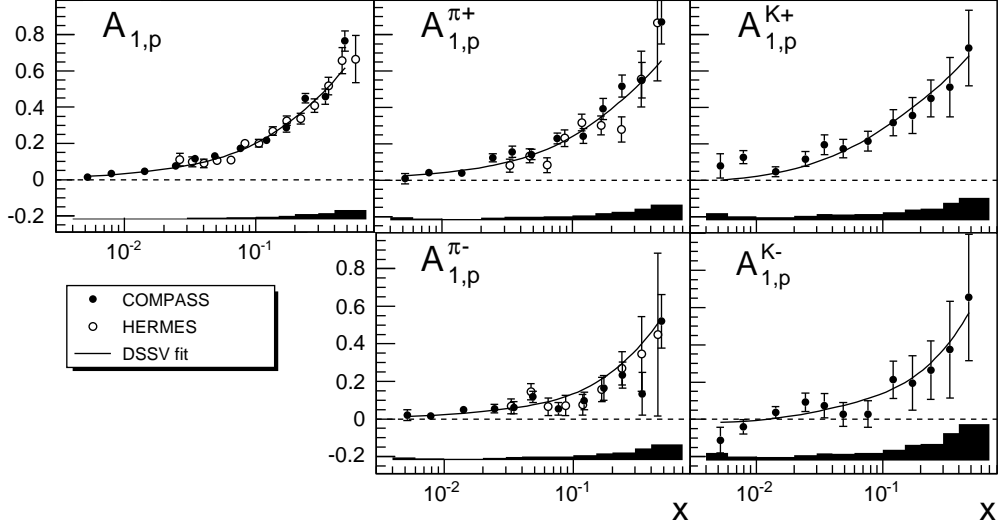


Fig. 6. – Proton asymmetries [2] compared to HERMES results [4] and the DSSV fit [5].

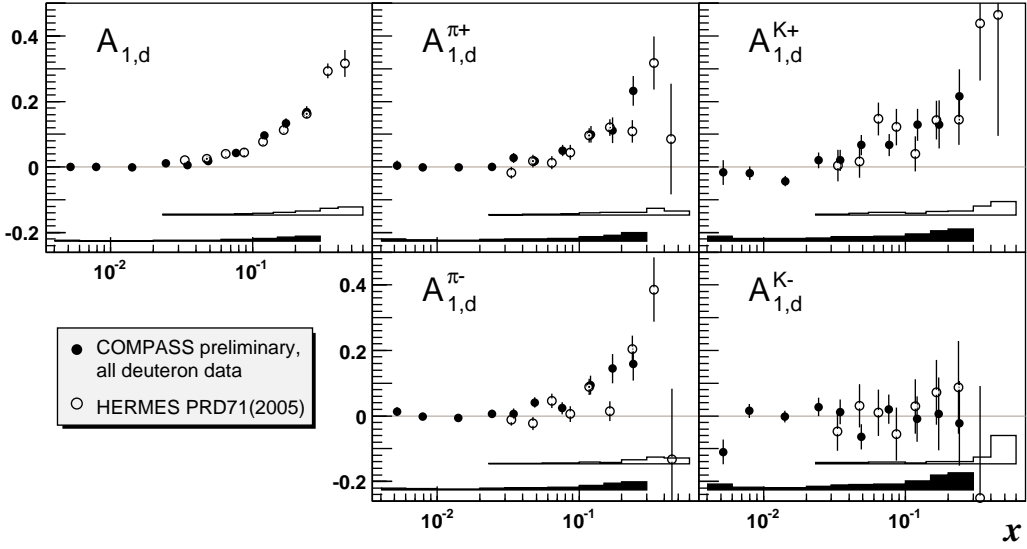


Fig. 7. – Deuteron asymmetries [3] compared to HERMES results [6].

the sea quark distributions vanish in this region. The result is summarised in table II and compared to the DSSV fit. The sum of all quark contributions $\Delta\Sigma = \sum_q \Delta q$ obtained from the semi-inclusive COMPASS data as $0.32 \pm 0.03 \pm 0.03$ agrees very well with the inclusive COMPASS result from g_1^d of $a_0 = 0.33 \pm 0.03$ [8]. The DSSV fit yields a considerably smaller value of $0.22 \pm 0.03 \pm 0.03$. The observed difference comes mainly

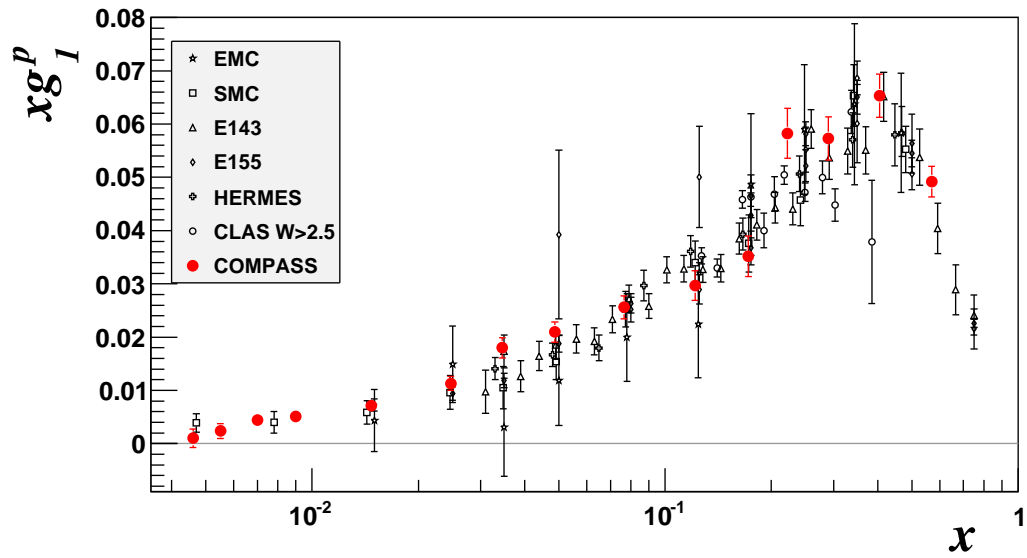


Fig. 8. – Proton structure function xg_1 as function of x at the Q^2 of the measurement.

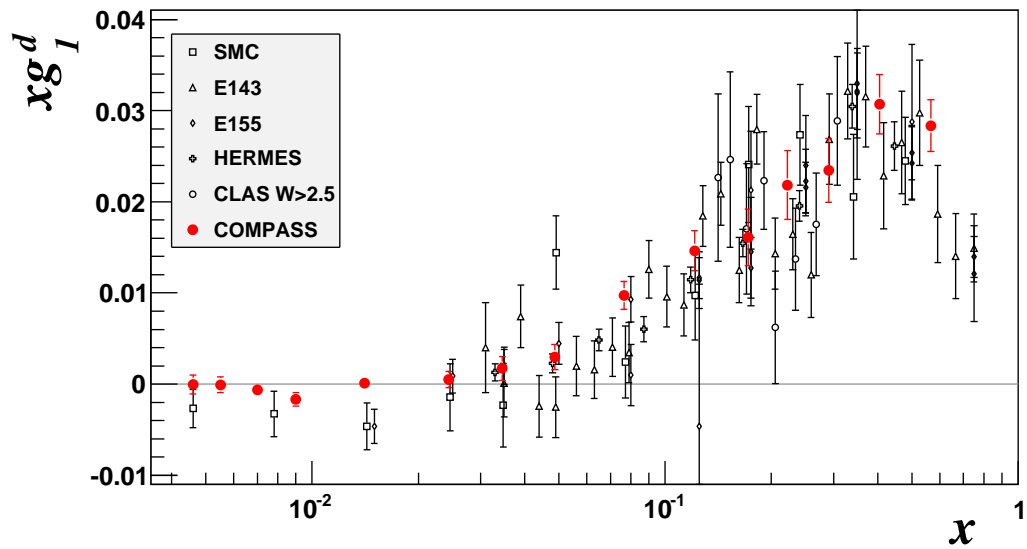


Fig. 9. – Deuteron structure function xg_1 as function of x at the Q^2 of the measurement.

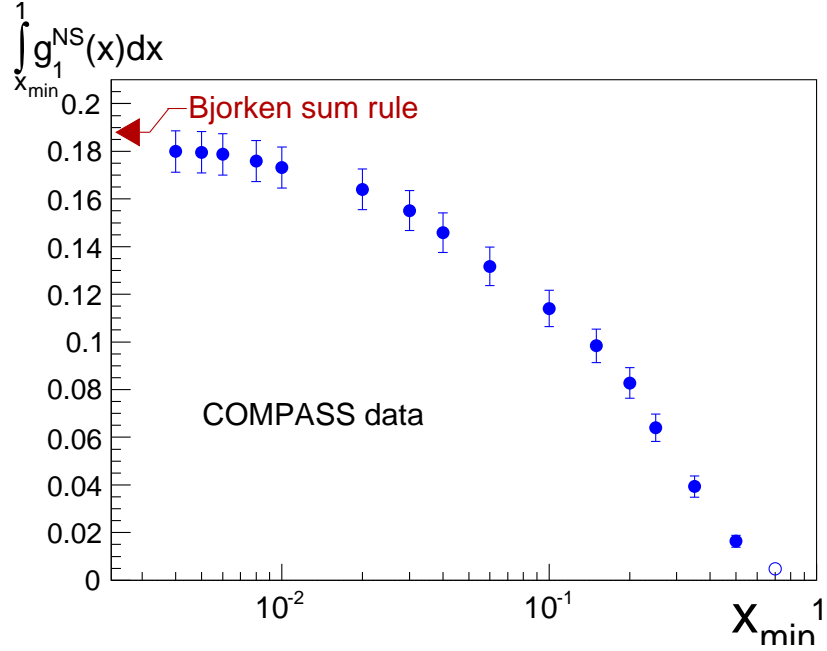


Fig. 10. – Integral $\int_{x_{\min}}^1 g_1^{NS}(x) dx$ of the non-singlet structure function g_1^{NS} as function of the lower integration limit x_{\min} .

from the negative behaviour of $\Delta s(x)$ assumed at small x . It should be noted that the results for $\Delta s(x)$ crucially depend on the used fragmentation functions as illustrated in ref. [2]. From the new, preliminary hadron multiplicities for an isoscalar target (fig. 12) it is obvious that fragmentation into (negative) kaons is not described well by the DSS [7] fragmentation functions, which were used both in the COMPASS analysis and in the DSSV fit. This casts some doubt on the reliability of the present determinations of the strange quark polarisation from semi-inclusive data. More data and further work on the fragmentation functions is required.

3.2. Gluons. – Following the discovery of the small quark spin contribution to the nucleon spin, a scenario was put forward, where the gluon spin masks the contribution of the quark spins via the axial anomaly. Even values of $6\hbar$ for $\Delta g = \int_0^1 g(x) dx$ were proposed [10]. With more data and slightly increasing quark spin contribution, the value for Δg dropped to about $2\hbar$, still four times the nucleon spin. A large negative orbital angular momentum L_z is required in this scenario to restore the nucleon spin of $1/2(\hbar)$

$$(5) \quad \frac{1}{2} = \frac{1}{2}\Delta\Sigma + \Delta g + L_z.$$

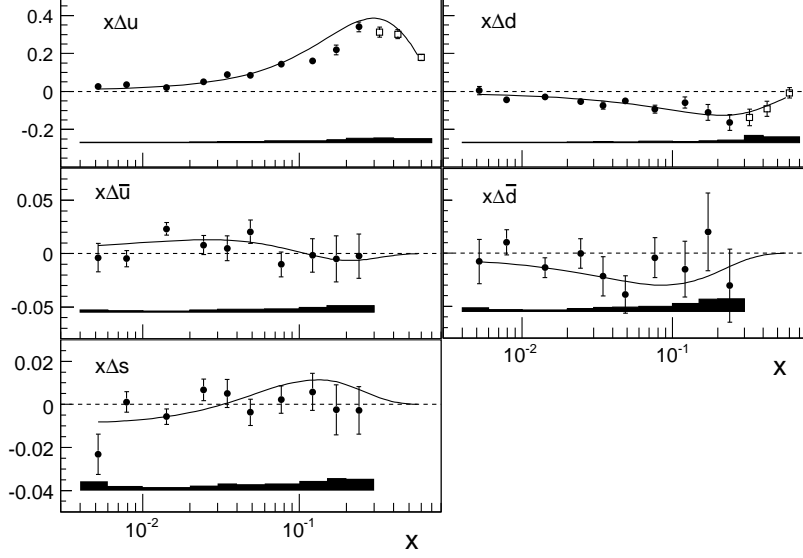


Fig. 11. – The quark helicity distributions $x\Delta u$, $x\Delta d$, $x\Delta\bar{u}$, $x\Delta\bar{d}$ and $x\Delta s$ at $Q_0^2 = 3 \text{ GeV}^2$ as a function of x . The values for $x < 0.3$ (black dots) are derived at LO from the COMPASS spin asymmetries using the DSS fragmentation functions [7]. Those at $x > 0.3$ (open squares) are derived from the values of the polarised structure function $g_1(x)$ quoted in [8, 9] assuming $\Delta q = 0$. The bands at the bottom of each plot show the systematic errors. The curves show the predictions of the DSSV fit calculated at NLO [5].

TABLE II. – Full first moments of the quark helicity distributions at $Q_0^2 = 3 \text{ GeV}^2$. The unmeasured contributions at low and high x were estimated by extrapolating the data towards $x = 0$ and $x = 1$ and by using the DSSV parametrisation [5]

	extrapol. full moment	DSSV
Δu	$0.71 \pm 0.02 \pm 0.03$	$0.71 \pm 0.02 \pm 0.03$
Δd	$-0.34 \pm 0.04 \pm 0.03$	$-0.35 \pm 0.04 \pm 0.03$
$\Delta\bar{u}$	$0.02 \pm 0.02 \pm 0.01$	$0.03 \pm 0.02 \pm 0.01$
$\Delta\bar{d}$	$-0.05 \pm 0.03 \pm 0.02$	$-0.07 \pm 0.03 \pm 0.02$
$\Delta s(\Delta\bar{s})$	$-0.01 \pm 0.01 \pm 0.01$	$-0.05 \pm 0.01 \pm 0.01$
Δu_v	$0.68 \pm 0.03 \pm 0.03$	$0.68 \pm 0.03 \pm 0.03$
Δd_v	$-0.29 \pm 0.06 \pm 0.03$	$-0.28 \pm 0.06 \pm 0.03$
$\Delta\Sigma$	$0.32 \pm 0.03 \pm 0.03$	$0.22 \pm 0.03 \pm 0.03$

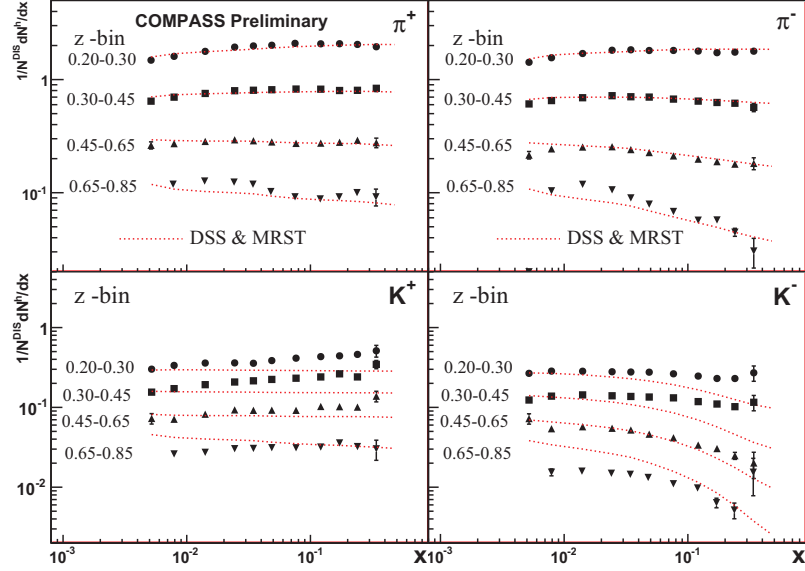


Fig. 12. – Preliminary hadron multiplicities from COMPASS for π^+ , π^- , K^+ and K^- as a function of x in various z bins. The curves are obtained with the DSS fragmentation functions and MRST04 PDFs.

The gluon polarisation can be determined from scaling violations in the spin-dependent structure function g_1 . However, the present range in Q^2 is insufficient to obtain $\Delta g(x)$ or its first moment with a sufficient precision. In SIDIS one has a direct handle on the gluon polarisation via the photon–gluon fusion (PGF) process (fig. 13). The measured cross-section asymmetry for PGF events is directly proportional to the gluon polarisation

$$(6) \quad A_1^{PGF} \propto \langle \hat{a}_{PGF} \rangle R_{PGF} \langle \Delta g/g \rangle$$

averaged over the covered range in the gluon momentum fraction x_g . However, there are competing processes yielding the same final state as PGF. Therefore Monte Carlo simulations are required in order to determine the fraction of PGF events R_{PGF} in the sample as well as the average analysing power $\langle \hat{a}_{PGF} \rangle$ of the hard process. At COMPASS the following final states were studied:

- pairs of light hadrons with high transverse momentum p_T with respect to the virtual photon in events with $Q^2 > 1 \text{ GeV}^2$ (LO) ([11] and preliminary results),
- pairs of light hadrons with high- p_T in events with $Q^2 < 1 \text{ GeV}^2$ (LO) [12],
- single charmed mesons (D^0, D^*) (LO) ([13] and preliminary LO, NLO results),
- single hadrons in events with $Q^2 < 1 \text{ GeV}^2$ (NLO, in preparation)

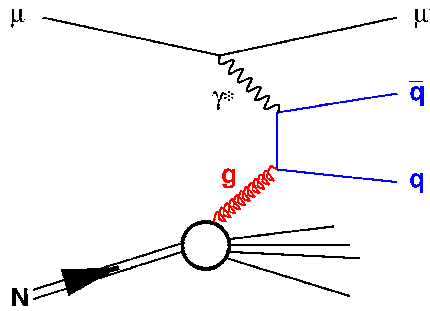


Fig. 13. – Sketch of the photon–gluon fusion process.

The cleanest of these processes is open-charm production via PGF because there is basically no physics background. The D^0 meson is identified via its decay $D^0 \rightarrow K^+\pi^- + c.c.$ The cross-section is small and combinatorial $K\pi$ background is large. Looking however at D^0 from $D^{*+} \rightarrow D^0\pi_s^+ + c.c.$, the situation improves drastically due to the additional detection of the slow π_s (fig. 14).

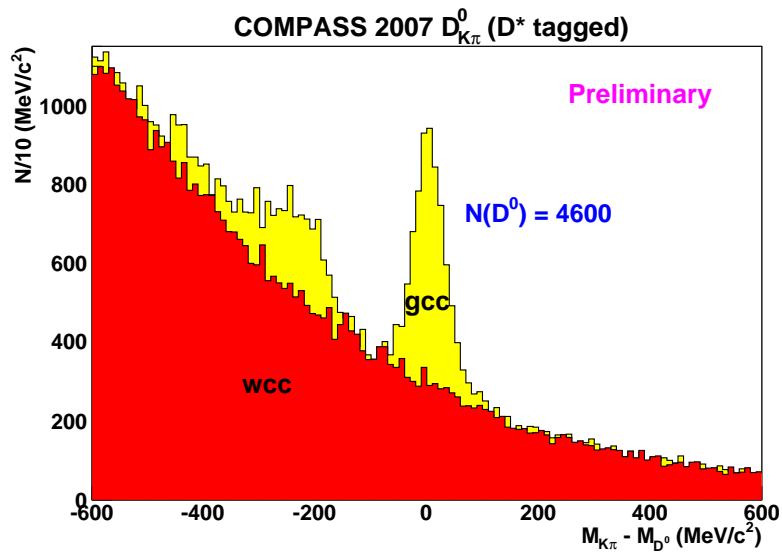


Fig. 14. – Mass spectrum of reconstructed D^0 mesons from D^* decay. Also shown is the combinatorial background of $K\pi$ pairs with wrong charge combination ('wcc', red). The structure left of the D^0 peak is a reflection of the $D^0 \rightarrow K\pi\pi^0$ decay, which can also be used in the determination of the gluon polarisation (preliminary 2007 data).

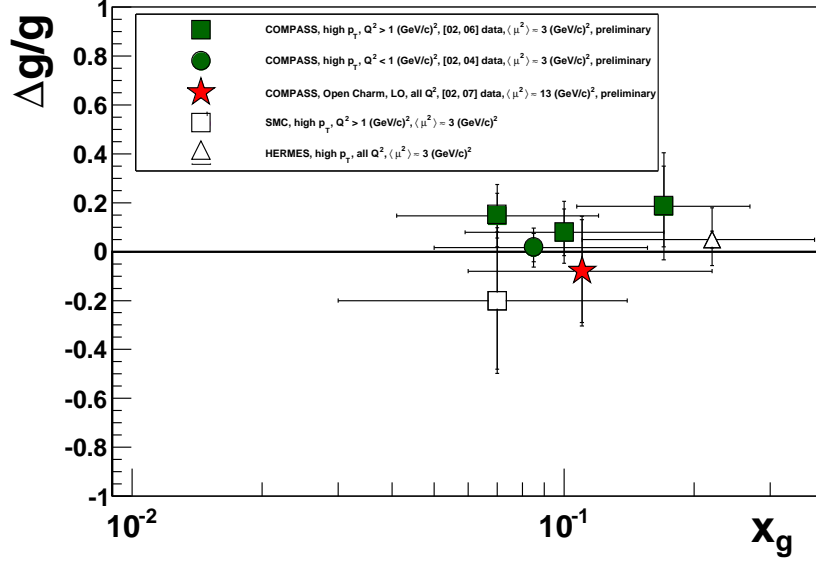


Fig. 15. – LO results for $\Delta g/g$ from analyses of hadron production via PGF as function of the gluon momentum fraction x_g .

In light-hadron production contributions from leading-order scattering and QCD-Compton processes are much larger and thus R_{PGF} is smaller. The stronger dependence on Monte Carlo simulations introduces a larger model dependence, which can however be controlled. All COMPASS LO results for the gluon polarisation are in agreement and shown in fig. 15 together with results from SMC and Hermes. A preliminary NLO analysis of the open-charm data yields $\Delta g/g|_{\text{NLO}} = -0.20 \pm 0.21$ (stat.) ± 0.08 (syst.). The main effect in going from LO to NLO is a shift of the average probed gluon momentum fraction x_g to larger values $\langle x_g \rangle = 0.28^{+0.19}_{-0.10}$. All results for the gluon polarisation are small, but nevertheless a significant contribution to the nucleon spin of $1/2\hbar$ can not be excluded. However, scenarios with gluon polarisations in the order of several \hbar are ruled out, a finding also confirmed by the RHIC experiments in polarised pp collisions.

Finally, COMPASS is working in collaboration with theorists on an analysis of single-hadron production in analogy to the RHIC π^0 analysis at much higher energies. A first result indicates that this method is applicable at COMPASS energies as well. In fig. 16 the agreement of the preliminary analysis and calculations is shown for three scales $\mu = p_T/2$, $\mu = p_T$ and $\mu = 2p_T$. For the smallest scale excellent agreement between data and theory is observed over almost five orders of magnitude. However, the small scale and the rather large scale dependence ask for further improvements on the theory side. Nevertheless, it

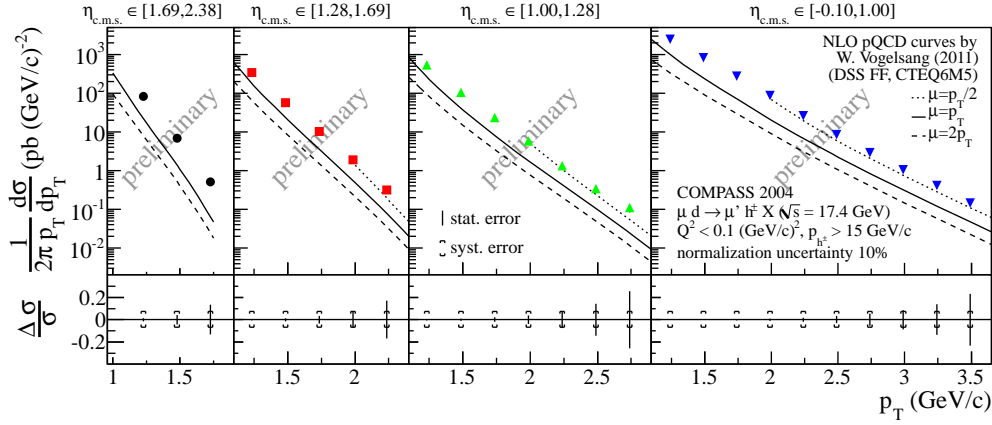


Fig. 16. – Cross-section as function of the transverse momentum of the produced hadron in three bins of the centre-of-mass pseudo-rapidity η . The curves show preliminary results of NLO resummed calculations by the W. Vogelsang, Tübingen.

is likely that from these data a precise and reliable determination of $\Delta g/g$ in NLO can be obtained in the future.

4. – Transverse spin structure results

Apart from the spin-averaged PDFs f_1 and the spin-dependent PDFs g_1 , a third structure function, h_1 or transversity, is needed to describe the nucleon at the twist-2 level. Like g_1 for the longitudinal case, h_1 describes the polarisation of quarks in the transverse case. Since h_1 is chiral odd, it needs to be coupled to a chiral-odd fragmentation function in order to appear in the photon–nucleon cross-section. There two such functions presently being used, the Collins function H_1^\perp for single hadrons and the interference fragmentation function (IFF) H_1^{\sphericalangle} for hadron pairs. Both lead to azimuthal cross-section asymmetries for scattering off transversely polarised targets.

The three PDFs mentioned above exhaust the information on nucleon structure at twist-2 if intrinsic transverse momenta k_T of quarks are integrated over. In total there are eight intrinsic-transverse-momentum (k_T) dependent PDFs at leading twist, all of which vanish upon integration apart of $f_1(x, k_T)$, $g_1(x, k_T)$ and $h_1(x, k_T)$ which reduce to the above mentioned PDFs. Of the TMD distributions the Sivers function f_{1T}^\perp and the Boer–Mulders function h_1^\perp are of particular interest. The former describes unpolarised partons in a transversely polarised nucleon, the latter transversely polarised partons in an unpolarised nucleon.

4.1. Transversity. – The azimuthal cross-section asymmetry $A_{UT} \propto A_C \sin \Phi_C$ generated by transversity and the Collins effect shows a $\sin \Phi_C$ dependence with an amplitude

of

$$(7) \quad A_C^h \propto \frac{\sum_q e_q^2 h_1^q(x) H_1^{\perp, h/q}(z, p_T)}{\sum_q e_q^2 f_1^q(x) D_1^{h/q}(z)},$$

where z is the energy fraction carried the hadron, p_T the hadron's transverse momentum and $D_1(z)$ the standard FF. The angle $\Phi_C = \phi_h - \phi_s - \pi$ is given by the azimuthal angles ϕ_h and ϕ_s of the hadron and the nucleon spin as defined in fig. 17.

A similar expression is obtained for the 2-hadron case with the IFF for the azimuthal cross-section asymmetry proportional to $A_{RS} \sin \phi_{RS} \sin \theta$

$$(8) \quad A_{RS}^h \propto \frac{\sum_q e_q^2 h_1^q(x) H_1^{\triangleleft, h/h/q}(z, M_{hh}^2)}{\sum_q e_q^2 f_1^q(x) D_1^{h/h/q}(z, M_{hh}^2)}.$$

Here $H_1^{\triangleleft}(z, M^2)$ and $D_1(z, M^2)$ denote the 2-hadron spin-dependent and spin-independent fragmentation functions, respectively. The angles are defined in fig. 18.

The preliminary results of the 2010 proton data for the Collins asymmetry are shown in fig. 19 (top). Large asymmetries of opposite sign are observed for positive and negative hadrons. Their magnitudes increase with x_B and exceed 5% at large x . The preliminary 2-hadron proton (2007) and deuteron (2002–2004) results are displayed in fig. 20 both for the deuteron (top) and the proton (bottom) [14]. As for the 2-hadron asymmetries, also the Collins asymmetries for the deuteron are compatible with zero (not shown here). This is an important result indicating that up and down quark transversity distributions have opposite sign.

4.2. Transverse-momentum dependent distributions. – The transverse-momentum (k_T) dependent Sivers function $f_{1T}^{\perp, q}(x, k_T)$ causes an azimuthal asymmetry

$$(9) \quad A_S^h \propto \frac{\sum_q e_q^2 f_{1T}^{\perp, q}(x, p_T/z) D_1^{h/q}(z)}{\sum_q e_q^2 f_1^q(x, p_T/z) D_1^{h/q}(z)},$$

which arises from a final state interaction. The cross-section asymmetry is proportional to $A_S \sin \Phi_S$, where the Sivers angle $\Phi_S = \phi_h - \phi_s$ is given by the difference of the azimuthal angles of the hadron and the spin vector as shown in fig. 17.

The latest COMPASS results for the proton are shown in fig. 19. A rather strong positive asymmetry is observed for positive hadrons increasing with x and reaching asymmetries of up to 4%. For negative hadrons the asymmetry is compatible with zero for $x < 0.1$ with an indication of an increasing asymmetry at the largest x values. There is a hint of decreasing Sivers asymmetry with increasing mass of the hadronic final state W . This trend first observed in the 2007 data [15] persists in the new 2010 data and might explain the somewhat larger asymmetries observed by HERMES[16].

For the deuteron the asymmetries appear to vanish over the full kinematic range accessible to COMPASS [17, 18] both for the Sivers and the Collins asymmetries. This

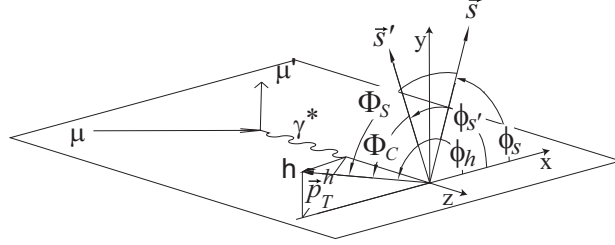


Fig. 17. – Definition of the Collins and Sivers angles. The vectors \vec{p}_T^h , \vec{s} and \vec{s}' are the hadron transverse momentum and the spin of the initial and struck quark, respectively.

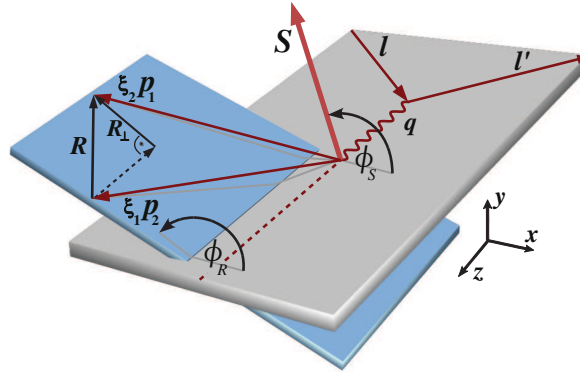


Fig. 18. – Definition of the azimuthal angles ϕ_R and ϕ_S for two-hadron production in deep inelastic scattering, where \mathbf{l} , \mathbf{l}' , \mathbf{q} and \mathbf{p}_i are the 3-momenta of beam, scattered muon, virtual photon and hadrons. Note that the azimuthal plane is defined by the directions of the relative hadron momentum and the virtual photon [14].

important result points to a cancellation of the up and down quarks asymmetries. All Collins and Sivers asymmetries were – or will be – also evaluated for identified pions and kaons.

Two preliminary spin-averaged asymmetries obtained for an unpolarised isoscalar target (${}^6\text{LiD}$) are shown in fig. 21. The upper $\cos\phi$ asymmetry is due to the Cahn effect and reaches almost 10% at large p_T . The lower $\cos 2\phi$ asymmetry originates from the Boer–Mulders TMD distribution describing transversely polarised partons in an unpolarised nucleon. Large asymmetries are observed – this time at small x_B – despite the fact that it is a deuteron-like target, where most of the other asymmetries are suppressed. The $\sin\phi$ asymmetry (not shown), however, is small.

5. – COMPASS plans for the future

The COMPASS Collaboration submitted in 2010 a proposal for new measurements to the CERN programme committee (SPSC) [19]. The proposal was approved in December

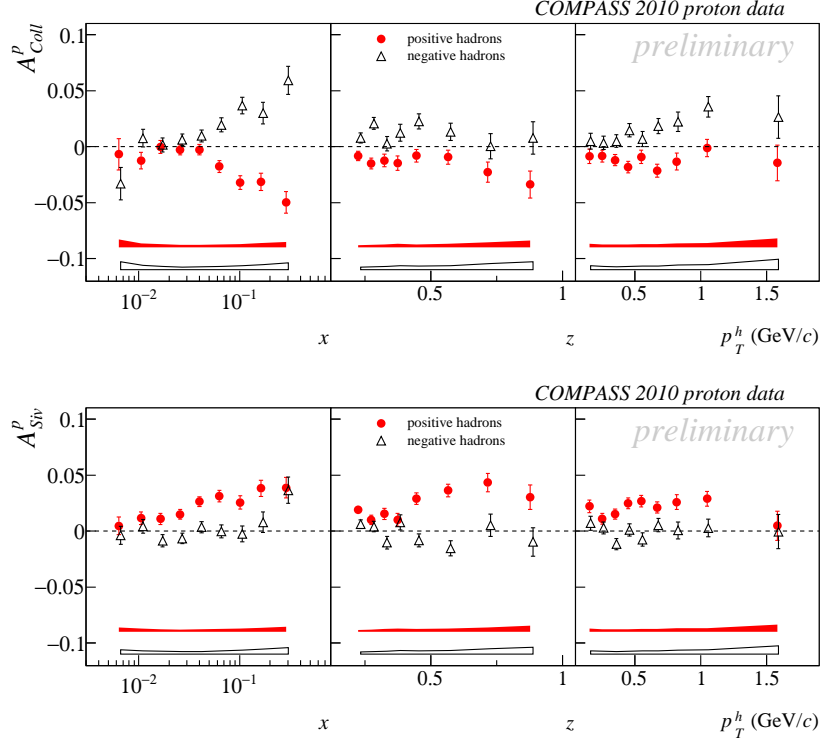


Fig. 19. – Preliminary Collins (top) and Sivers (bottom) asymmetries for the proton as function of x , z and p_T from the 2010 data.

2010 and experiments will start in 2012 with a pion/kaon polarisability measurement (not discussed here). The future programme starting 2014 after the accelerator shutdown focuses on TMD distributions and GPDs. A polarised Drell–Yan experiment will take place in 2014 and in 2015/2016 deeply virtual Compton scattering (DVCS) and hard exclusive meson production (HEMP) will be studied with an unpolarised target. A pilot run for the latter experiment is planned already for late 2012. In parallel with the GPD programme high statistics SIDIS data will be taken.

5.1. GPD programme. – The novel concept of generalised parton distributions is by now well established and widely considered as the tool to get a more detailed understanding of how quark and gluons build up the nucleon. GPDs are universal distributions which contain as limiting cases nucleon form factors on the one hand and PDFs on the other. The distributions H^f and \tilde{H}^f ($f = u, d, s, g$) describe processes where the nucleon helicity is preserved and contain as limiting cases the PDFs f_1 and g_1 , respectively. Processes where the nucleon helicity is flipped are described by the GPDs E^f and \tilde{E}^f for which no such limiting case exists. GPDs correlate transverse spatial and longitudinal momentum

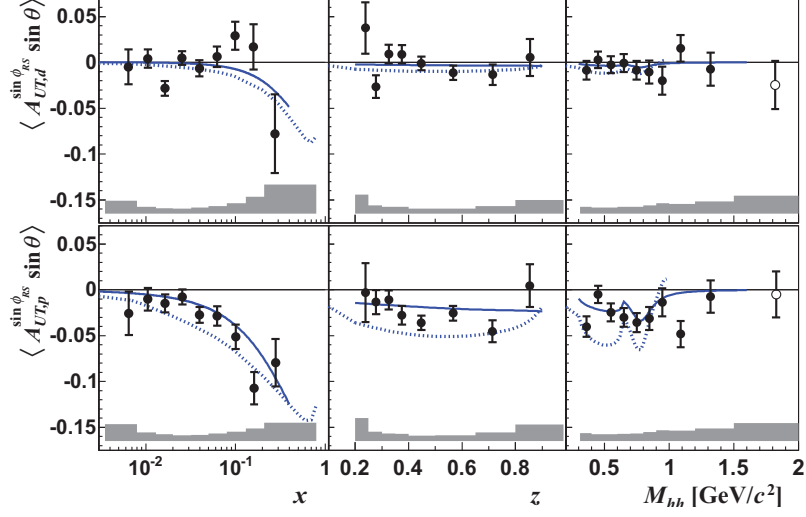


Fig. 20. – Deuteron (top) and proton (bottom) 2-hadron asymmetries, integrated over θ as a function of x , z , and M_{hh} . For details and the curves showing predictions see ref. [14].

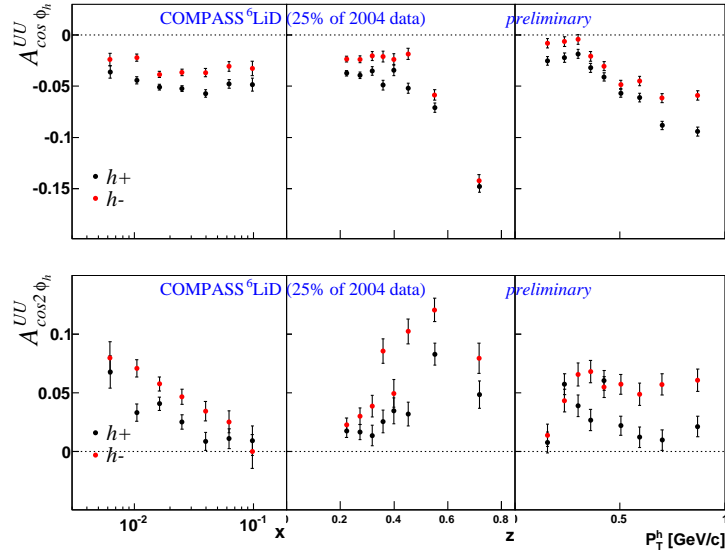


Fig. 21. – Cahn (top) and Boer–Mulders asymmetries for ${}^6\text{LiD}$ target and positive and negative hadrons as a function of x , z , and p_T^h . The kinematic factors are divided out.

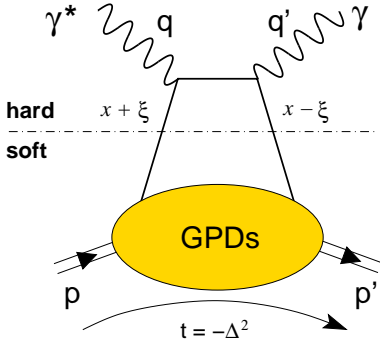


Fig. 22. – Handbag diagram for the DVCS process at leading twist.

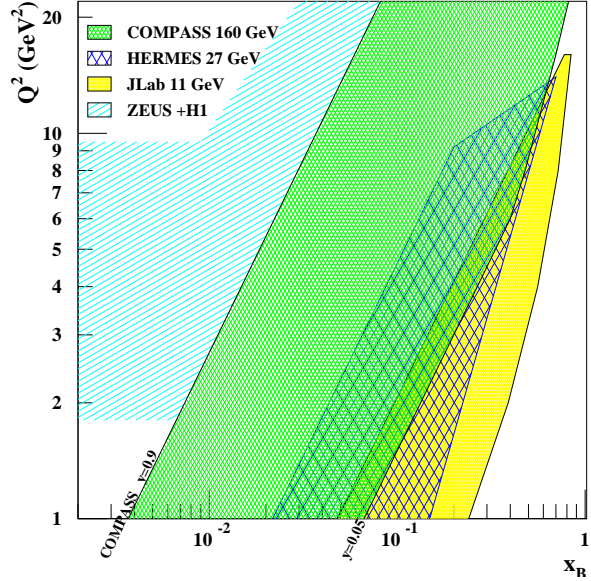


Fig. 23. – Kinematic domains for measurements of hard exclusive processes shown for the COMPASS (green area enclosed by the lines $y = 0.9$ and $y = 0.05$), HERMES and JLab fixed-target experiments and the HERA collider experiments H1 and Zeus.

and thus provide a kind of ‘nucleon tomography’. They depend on four variables x , ξ , t , and Q^2 . The cleanest process to assess GPDs is DVCS shown in fig. 22, which also defines the relevant momentum fractions, x (not the Bjorken scaling variable) and ξ , and the momentum transfers, t and Q^2 . The former two variables represent respectively average and half the difference between the initial and final longitudinal momentum fractions of the nucleon, carried by the parton throughout the process. The Bjorken scaling variable x_B is in this kinematics related to the skewness as $\xi \simeq x_B / (2 - x_B)$ in the Bjorken limit.

The interest in these distributions was boosted, when X.-D. Ji showed that there is a sum rule for the total angular momentum J^f of a quark or a gluon and the corresponding GPDs [20]

$$(10) \quad J^f(Q^2) = \frac{1}{2} \lim_{t \rightarrow 0} \int_{-1}^1 dx x [H^f(x, \xi, t, Q^2) + E^f(x, \xi, t, Q^2)],$$

which holds for any value of ξ . Knowing the quark spin contribution to the nucleon spin, one can – in principle – determine the orbital angular momentum contribution. This is presently the only unambiguous method to assess the angular orbital momentum and to solve the nucleon spin puzzle. However, an actual measurement will require a world-wide effort of various experiments. The kinematic domains of some experiments are displayed in fig. 23. COMPASS will explore the uncharted territory in between the collider region

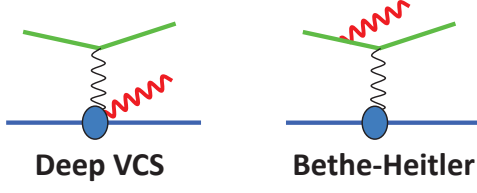


Fig. 24. – DVCS and Bethe–Heitler processes.

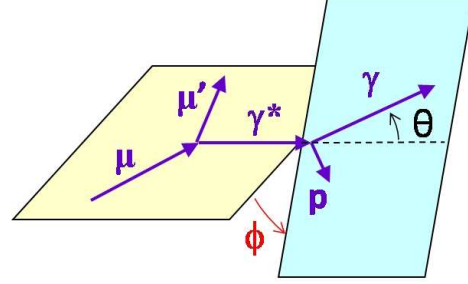


Fig. 25. – Definition of angles for the DVCS process.

and that of the lower-energy fixed-target HERMES and JLab experiments.

The DVCS process interferes with the Bethe–Heitler (BH) process due to identical final states (fig. 24). The cross-section then contains five terms

$$(11) \quad d\sigma^{\mu p \rightarrow \mu p \gamma} = d\sigma^{\text{BH}} + d\sigma_0^{\text{DVCS}} + P_\mu d\Delta\sigma^{\text{DVCS}} + e_\mu \Re I + P_\mu e_\mu \Im I,$$

where I denotes the DVCS–BH interference term. A characteristic feature of this cross-section is its ϕ dependence, the azimuthal angle between lepton scattering plane and real-photon production plane (fig. 25).

In 2009 COMPASS performed a preparatorial measurement with a 40 cm long liquid hydrogen target to validate the Monte Carlo simulations and to demonstrate the feasibility of the measurement. The result is shown in fig. 26. An important feature is that the normalisation can be fixed at small x_B , where the well-known BH process dominates. The observed ϕ distributions nicely match the MC prediction, although statistics is poor. In the largest x_B bin a clear contribution from DVCS is visible.

From eq. 11 one can build the sum \mathcal{S} and difference \mathcal{D} of the $\mu p \rightarrow \mu p \gamma$ cross-section for simultaneous change of lepton charge e_μ and polarisation P_μ of the incoming lepton beam (+ to – and \leftarrow to \rightarrow)

$$(12) \quad \begin{aligned} \mathcal{D} &= d\sigma^{\leftarrow} - d\sigma^{\rightarrow} = 2(d\sigma_0^{\text{DVCS}} + \Re I) \\ \mathcal{S} &= d\sigma^{\leftarrow} + d\sigma^{\rightarrow} = 2(d\sigma_0^{\text{BH}} + d\sigma_0^{\text{DVCS}} + \Im I). \end{aligned}$$

The muon beam used at COMPASS has exactly this behaviour that negative muons have opposite polarisation than positive muons due to the weak pion decay. Upon integration over the azimuthal angle ϕ (fig. 25) the interference contribution to \mathcal{S} vanishes [21] and after subtraction of the BH cross-section, one obtains the DVCS cross-section. This cross-section depends on the squared momentum transfer t from the initial to final nucleon (fig. 22). At small x_B one has the relation $\langle r_\perp^2(x_B) \rangle \approx 2B(x_B)$ if the exclusive cross-section is parametrised as $d\sigma/dt \propto \exp(-B(x_B)|t|)$. The transverse distance r_\perp is measured between the struck quark and the centre of mass of the spectator

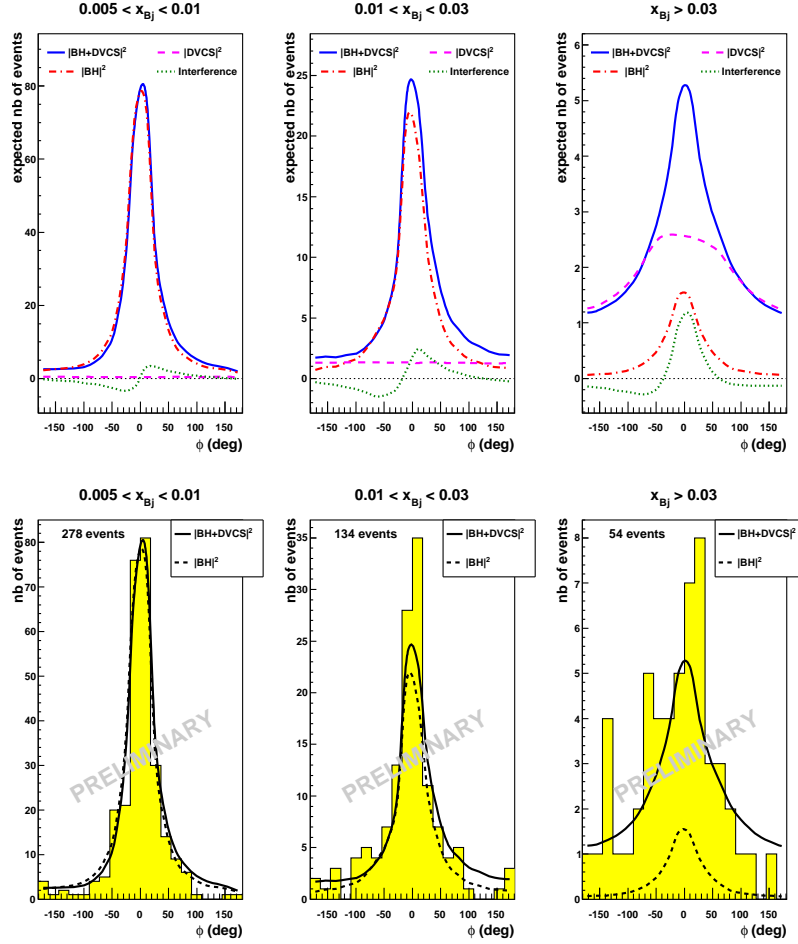


Fig. 26. – Event numbers as a function of ϕ for three bins in x_B obtained from a Monte Carlo simulation (top) and data from a test run in 2009 (bottom). The Monte Carlo simulation is normalised to the lower x_B bin where BH dominates. The curves in the lower plot are the same as the solid (total) and dash-dotted (BH) curves in the upper plot.

system. Thus, independent of any GPD parametrisation, one obtains a measure of the transverse nucleon size as a function of x_B . Using a parametrisation of the type $B(x_B) = B_0 + 2\alpha' \log(x_0/x_B)$, one can characterise the t slope of the cross-section by the parameter α' shown in fig. 27. The projected precision of a t -slope measurement is presented in fig. 27. A new electromagnetic calorimeter, ECAL0, will improve the precision of the measurement and enlarge the accessible range towards larger x_B . Combined with the HERA data and future JLab data a comprehensive picture of the evolution of the nucleon's transverse size with x_B will be achieved in a model-independent way. For

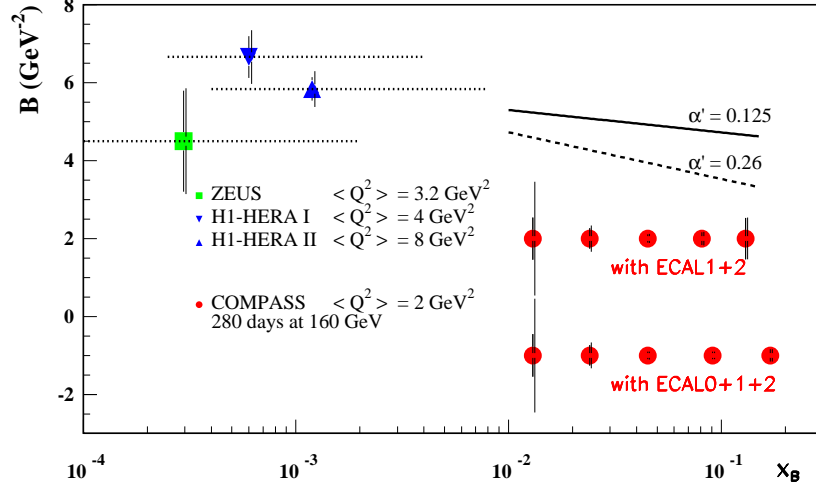


Fig. 27. – Projections for the measurement of the x_B dependence of the t -slope parameter $B(x_B)$ of the DVCS cross-section calculated for $1 \text{ GeV}^2 < Q^2 < 8 \text{ GeV}^2$ (red filled dots, right). The left vertical bar on the points indicates the statistical error only while the right one includes also the quadratically added systematic uncertainty, using only ECAL1 and ECAL2 (upper row) and also an additional ECAL0 calorimeter (lower row). For comparison some Hera results with similar $\langle Q^2 \rangle$ are also shown [22, 23]. Dashed horizontal lines indicate the x_B range of these measurements. Two different slopes are indicated for $\alpha' = 0.125 \text{ GeV}^2$ and 0.26 GeV^2 .

the 2012 pilot DVCS run we project already a significant measurement combining the three central x_B bins of fig. 27 into one large x_B .

For DVCS with $\xi = 0$ there is only a pure transverse momentum transfer $t = -\Delta_{\perp}^2$. The Fourier transform of the Δ_{\perp}^2 dependence of the GPD $H^f(x, 0, -\Delta_{\perp}^2)$ for fixed x describes the spatial distribution of partons of species f carrying the momentum fraction x . This is sketched in fig. 28. Here the impact parameter b is the transverse distance between the struck quark and the centre of mass of the whole nucleon. Thus for $x \rightarrow 1$ the distribution must shrink towards zero.

The ϕ dependence of the difference \mathcal{D} , the sum \mathcal{S} and the asymmetry $\mathcal{A} = \mathcal{D}/\mathcal{S}$ of the DVCS cross-sections defined in eq. 12 allow for the extraction of quantities related to Compton form factors (CFF) which in turn depend on the GPDs. With an unpolarised target, COMPASS DVCS results will mainly provide information on the CFF \mathcal{H} and thus constrain the GPD H . For details of the ϕ dependence see ref. [19] and references therein. Results will be obtained in (x_B, Q^2) bins. An example for the projected precision in such a bin is shown in fig. 29 for the beam charge-and-spin asymmetry \mathcal{A} .

Some handle on the flavour separation of GPDs may be obtained from measurements of hard exclusive meson production, where the meson replaces the real photon of DVCS. Contrary to the DVCS case, gluon GPDs contribute in leading order in HEMP and BH interference does not exist. It is foreseen to measure cross-sections for a large set of

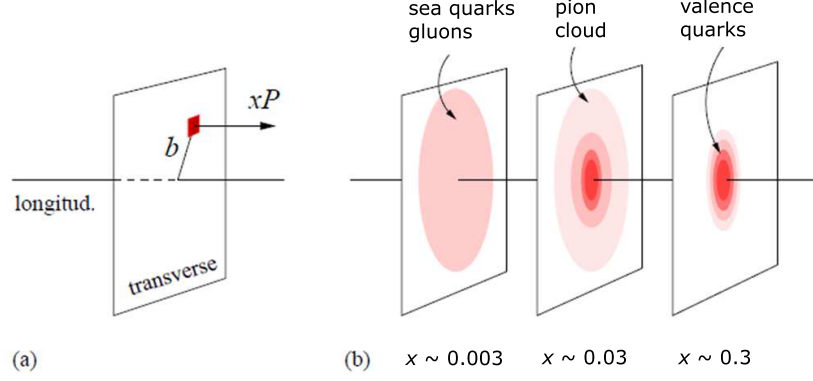


Fig. 28. – Nucleon tomography. a) The Fourier transform of the $-\Delta_{\perp}^2$ dependence of the GPD $H^f(x, 0, -\Delta_{\perp}^2)$ for fixed x describes the distribution of the transverse distance $b \equiv |\mathbf{b}_{\perp}|$ of partons, carrying the fraction x of the nucleon’s longitudinal momentum P , from the centre of momentum of the nucleon. b) Sketch of tomographic views of the transverse spatial parton distribution in the nucleon at certain parton longitudinal momentum fractions x . Figure adapted from ref. [24].

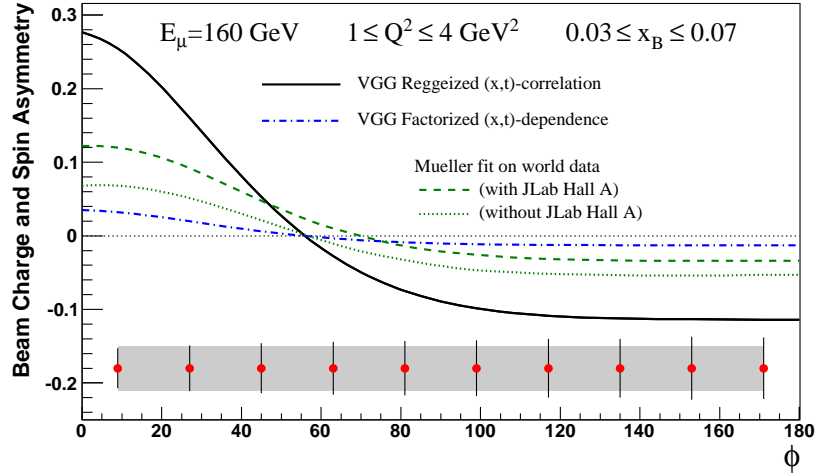


Fig. 29. – Projected statistical accuracy for a measurement of the dependence of the beam charge-and-spin asymmetry on ϕ . As an example the 2-dimensional bin $0.03 < x_B < 0.07$ and $1 \text{ GeV}^2 < Q^2 < 4 \text{ GeV}^2$ is shown. Predictions are calculated using the VGG model [25]. The black (solid) and blue (dash-dotted) curves correspond to two different variants of this model. The green curves show predictions based on the first fit of world data [26] including JLab Hall A (dashed line) or not (dotted line).

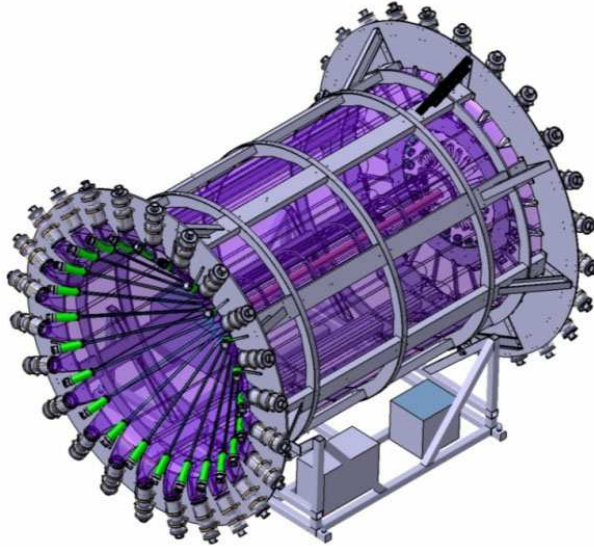


Fig. 30. – The Camera recoil detector.

mesons (π , η , ρ , ω , ϕ , J/ψ , ...), which are all sensitive to different combinations of quark and gluon GPDs. The GPD E can in principle be assessed using a transversely polarised target. Such measurements are under consideration for a later stage of the programme.

Another physics topic, which will be pursued in parallel with DVCS, is the study of spin-independent TMD distributions like the Boer–Mulders distribution and of fragmentation functions, in particular for strange quarks. Also the spin-averaged strange quark PDF needs further studies. Up to now COMPASS used polarised NH_3 and ${}^6\text{LiD}$. With the liquid hydrogen target a clean unpolarised proton measurement will be possible for the first time in COMPASS.

A major rearrangement of the spectrometer target region will be necessary for the GPD measurements. The polarised target has to be removed and a recoil proton detector, the Camera detector, will be installed. It consists of two concentric scintillator barrels of 3.6 m length and 2.2 m diameter for the outer barrel (fig. 30). The photomultiplier signals will be digitised with 1 GHz to cope with the high rate and pile-up. Camera is essential to ensure the exclusivity of the observed reactions. It houses on the central axis a 2.5 m long liquid hydrogen target. In order to improve the acceptance of real photons, a third electromagnetic calorimeter, ECAL0, will be constructed and placed just downstream of the Camera detector. Multipixel avalanche photodiodes were chosen for the readout to avoid problems due the magnetic field of the close spectrometer magnet SM1. For the pilot run in 2012 the Camera detector and part of ECAL0 will be available. It is also planned to replace the MWPCs photodetectors of the RICH by a new system based on

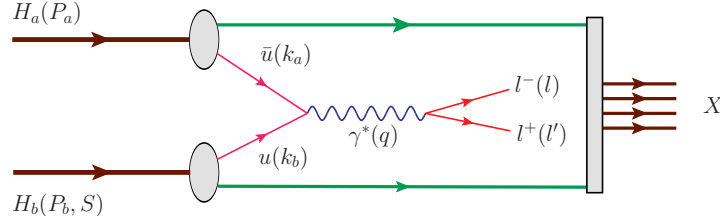


Fig. 31. – Sketch of the Drell-Yan process. A quark and antiquark from target and projectile fuse into a virtual photon decaying into a $\mu^+\mu^-$ pair.

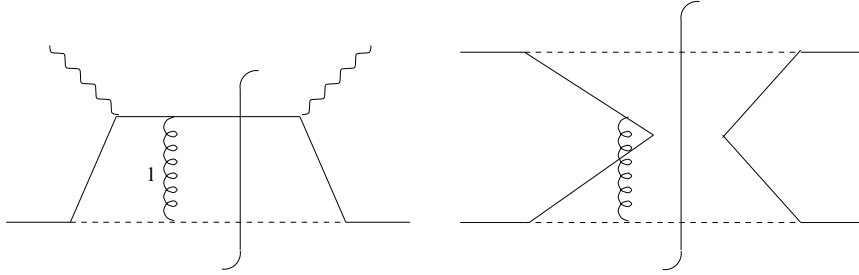


Fig. 32. – Graph for single-spin asymmetries for SIDIS (left) and DY (right) from ref. [27].

thick GEMs with CsI coating. This is in particular important for the HEMP and FF measurements.

5.2. Drell-Yan programme. – The second approach to the transverse nucleon structure in the future COMPASS programme is via the Drell-Yan process shown in fig. 31. The advantage in DY processes is that fragmentation functions are not involved. However, this has to be paid by a convolution of two distribution functions. A completely symmetric situation is the scattering of a polarised antiproton off a polarised proton. A more accessible option which in addition guarantees high luminosity is pion-proton scattering. A negative pion contains an anti-up-quark as valence quark, just like an antiproton. The DY process then proceeds via the fusion of an anti-up-quark from the pion and a up quark from the proton and the cross-section is given by $\sigma^{\text{DY}} \propto \sum_f f_{\bar{u}|\pi^-} \otimes f'_{u|p}$, where f and f' are generic place holders of PDFs. The process is strongly dominated by the up quark distributions.

Using a transversely polarised proton target, one can study TMD distributions like the Sivers and Boer-Mulders distributions. Theory predicts that these naive T-odd TMD distributions obey only a restricted universality. Contrary to normal PDFs they should change sign when observed in SIDIS and DY, respectively.

$$(13) \quad f_{1T}^\perp|_{\text{DY}} = -f_{1T}^\perp|_{\text{DIS}} \quad \text{and} \quad h_1^\perp|_{\text{DY}} = -h_1^\perp|_{\text{DIS}}.$$

TABLE III. – *Future Drell–Yan experiments*

Facility	Type		s (GeV ²)	Time-line
RHIC (STAR, PHENIX)	collider,	$p^\uparrow p^\uparrow$	$200^2, 500^2$	> 2015
RHIC(internal target)	fixed target,	$p^\uparrow p^\uparrow$	500	> 2016
RHIC(AnDY)	collider,	$p^\uparrow p^\uparrow$	500^2	> 2013
JPARC	fixed target,	pp^\uparrow	$60 \div 100$	> 2017
GSI(PAX)	collider,	$\bar{p}^\uparrow p^\uparrow$	200	> 2020
GSI (Panda)	fixed target,	$\bar{p}p$	30	> 2017
NICA	collider,	$p^\uparrow p^\uparrow, d^\uparrow d^\uparrow$	676	> 2017
COMPASS	fixed target,	$\pi^- p^\uparrow$	$300 \div 400$	2014

This sign change is due to going from a final-state interaction in SIDIS to an initial-state interaction in DY (fig. 32) [27]. A violation of this prediction would imply drastic consequences on how cross-sections are calculated in QCD. Therefore it has generated wide-spread interest in a direct comparison of TMD distributions obtained from SIDIS and DY, respectively. Plans for future polarised DY experiments exist at various laboratories (table III). The COMPASS DY experiment is planned and approved for 2014. It will use a 190 GeV negative pion beam and a transversely polarised proton (NH₃)

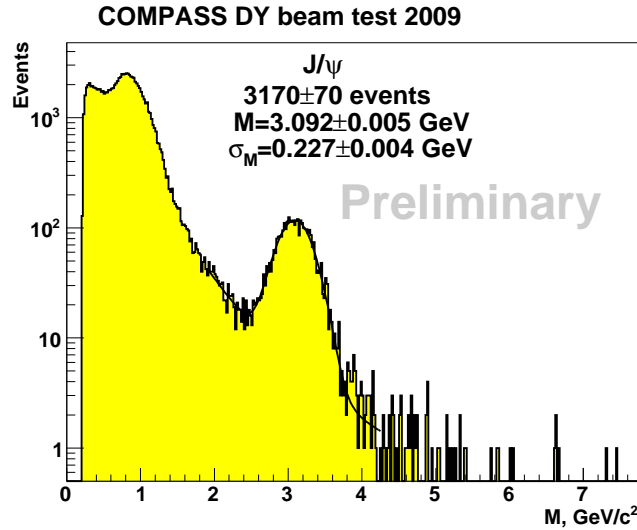


Fig. 33. – Event numbers versus the dimuon mass from a short beam test in 2009. The save region is above 4 GeV, away from the prominent J/ψ peak.

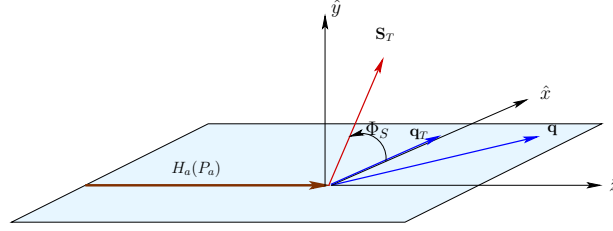


Fig. 34. – Definition of the azimuthal angle ϕ_S of transverse target spin \mathbf{S}_T in the target rest frame.

target. The measurement will primarily assess transversity h_1 and the T-odd Sivers and Boer–Mulders TMD distributions, f_{1T}^\perp and h_1^\perp for up quarks. For all of these COMPASS SIDIS measurements exist, showing non-vanishing asymmetries for the proton.

To avoid the J/ψ region and the region of background from charm decays, the experiments will focus on dimuon masses $4 \text{ GeV} < M_{\mu\mu} < 9 \text{ GeV}$. The region below the J/ψ mass, $2 \text{ GeV} < M_{\mu\mu} < 2.5 \text{ GeV}$, will also be studied but analysis will be more involved. Here the signal-to-background ratio will be unfavourable, in the order of unity. A first dimuon mass spectrum taken in a short test run in 2009 is shown fig. 33.

The measurable azimuthal asymmetries depend on the angles ϕ_S and ϕ defined in fig. 34 and on the Feynman variable $x_F = x_\pi - x_p$, where x_π and x_p are the momentum fractions carried by the involved quarks in the pion and proton, respectively. The COMPASS acceptance in the (x_π, x_p) plane is shown in fig. 35. It is large for $x_F > 0$ and reaches about 50 % at $x_F \approx 0.4$. The projected $A_T^{\sin \phi_S}$ asymmetry measurement in the high-mass region $4 \text{ GeV} < M_{\mu\mu} < 9 \text{ GeV}$ is compared to predictions in fig. 36. The planned measurement will certainly be able to answer the sign question of T-odd TMD distributions and allow for a comparison of the absolute size of the effects in SIDIS and DY. However, a determination of the shape of the Sivers TMD distribution in DY will only be possible in the less clean low-mass range (fig. 37 left) or with further measurements. The shaded grey area and the central line in figs. 36 and 37 correspond to a calculation based on a TMD PDF fit to data [28]. For the other curves see ref. [19]. The Boer–Mulders related asymmetry $A_T \cos 2\phi$ will be determined with high precision in both the low and high-mass regions.

Major modifications will be required to the COMPASS spectrometer for the DY measurements. As the measurement is statistics limited optimising the luminosity is mandatory. This in turn brings up serious radiation and detector occupancy issues, which can be solved using a massive hadron absorber downstream of the target. The polarised target has to be moved upstream with all attached services by about 3 m to create space for the absorber as shown in fig. 38. The absorber itself will consist of a tungsten core surrounded by alumina (Al_2O_3) and concrete blocks. Alumina was chosen to minimise multiple scattering. This is an essential element to disentangle the oppositely polarised target cells in the track reconstruction. On the downstream side a stainless steel section

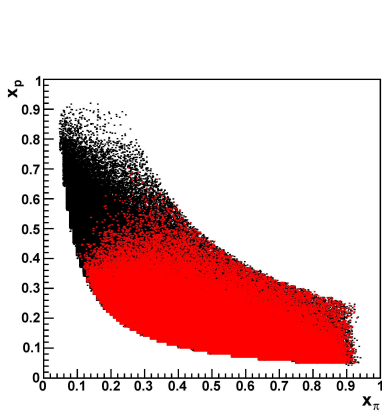


Fig. 35. – Covered kinematic region in x_π vs x_p for a dimuon mass $4 \text{ GeV} < M_{\mu\mu} < 9 \text{ GeV}$.

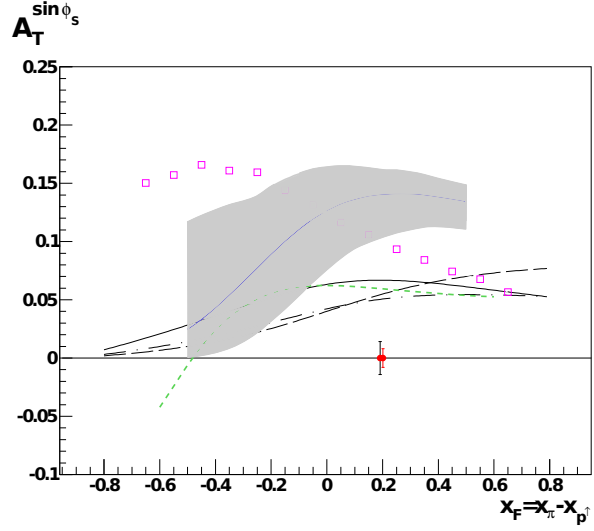


Fig. 36. – Theoretical predictions and expected statistical (left) and systematic (right) error for a measurement of the Siverts asymmetry in the high-mass region.

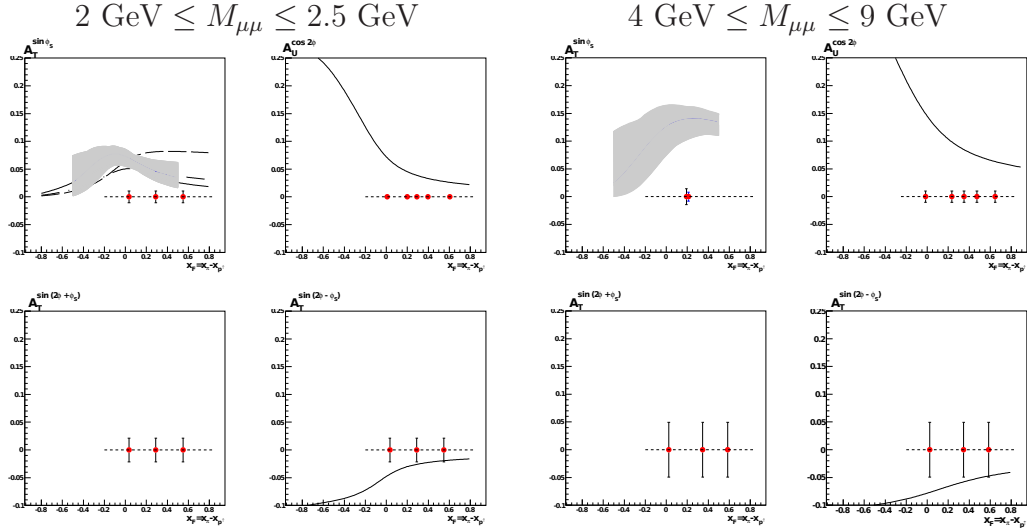


Fig. 37. – Projections for measurements of the $A_T^{\sin \phi_S}$ (Siverts), $A_U^{2\cos \phi_S}$ (Boer–Mulders), $A_T^{\sin(2\phi+\phi_S)}$ and $A_T^{\sin(2\phi-\phi_S)}$ asymmetries for the low-mass region (left) and the high-mass region (right) as a function of the variable $x_F = x_\pi - x_p$.

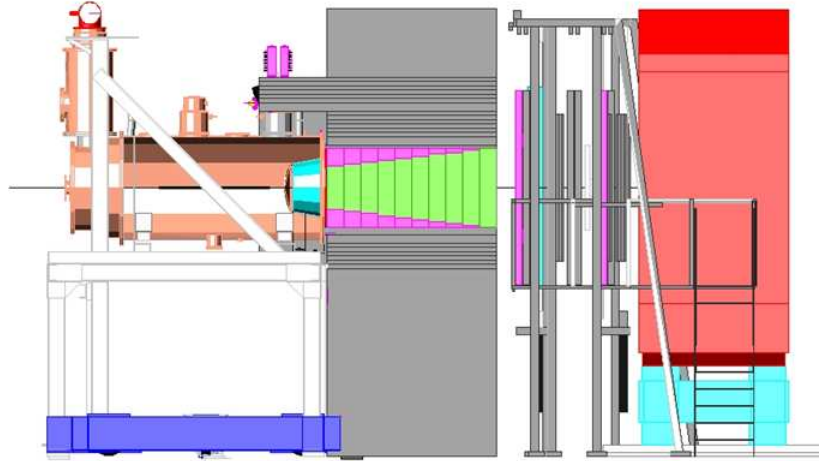


Fig. 38. – Layout of the target region for the DY measurement. The polarised target left is followed by massive hadron absorber. To the right the tracking stations and the first spectrometer (red) are shown.

will replace the alumina part.

6. – Summary

After the measurement of the pion polarisability in 2012 and the accelerator shutdown in 2013, COMPASS will focus on the 3-dimensional and transverse structure of the nucleon. In a pilot GPD run at the end of 2012 first data will be collected and a result for the t slope of the ϕ -integrated deeply-virtual-Compton-scattering cross-section be obtained.

The year 2014 will be dedicated to the Drell-Yan measurement with a negative pion beam and a transversely polarised proton target. This will bring the first result for the size and the sign of the T-odd TMD distributions in Drell-Yan reactions. In 2015 and 2016 the production runs for the GPD measurement with a pure liquid hydrogen target will take place, comprising deeply virtual Compton scattering and hard exclusive meson production. Simultaneously, data on the spin-independent TMD distributions and on fragmentation functions will be taken. With this programme COMPASS will continue to make major contributions to the field of nucleon structure.

Acknowledgements

I acknowledge the precious help of many COMPASS colleagues in preparing this lecture and thank the organisers for the inspiring school.

REFERENCES

- [1] COMPASS Collaboration, P. Abbon *et al.*, Nucl. Instrum. and Meth. **A577** (2007) 455.
- [2] COMPASS Collaboration, M. G. Alekseev *et al.*, Phys. Lett. **B693** (2010) 227.
- [3] COMPASS Collaboration, M. Alekseev *et al.*, Phys. Lett. **B680** (2009) 1.
- [4] HERMES Collaboration, A. Airapetian *et al.*, Phys. Rev. **D75** (2007) 012007.
- [5] D. de Florian, R. Sassot, M. Stratmann, W. Vogelsang, Phys. Rev. Lett. **101** (2008) 072001; Phys. Rev. **D80** (2009) 034030.
- [6] HERMES Collaboration, A. Airapetian *et al.*, Phys. Rev. **D71** (2005) 012003.
- [7] D. de Florian *et al.*, Phys. Rev. **D75** (2007) 114010.
- [8] COMPASS Collaboration, V. Yu. Alexakhin *et al.*, Phys. Lett. **B647** (2007) 8.
- [9] COMPASS Collaboration, M. G. Alekseev *et al.*, Phys. Lett. **B690** (2010) 466.
- [10] G. G. Ross, Univ. of Oxford preprint OUTP-89-39P, Aug. 1989.
- [11] COMPASS Collaboration, Ch. Adolph *et al.*, [hep-ex/1202.4064], subm. Phys. Lett. B.
- [12] COMPASS Collaboration, E. S. Ageev *et al.*, Phys. Lett. **B633** (2006) 25.
- [13] COMPASS Collaboration, M. Alekseev *et al.*, Phys. Lett. **B676** (2009) 31.
- [14] COMPASS Collaboration, C. Adolph *et al.*, arXiv:1202.6150 [hep-ex], subm. Phys. Lett. **B**.
- [15] COMPASS Collaboration, M. Alekseev *et al.*, Phys. Lett. **B692** (2010) 240.
- [16] HERMES Collaboration, A. Airapetian *et al.*, Phys. Rev. Lett. **103** (2009) 152002.
- [17] COMPASS Collaboration, E. S. Ageev *et al.*, Nucl. Phys. **B765** (2007) 31.
- [18] COMPASS Collaboration, M. Alekseev *et al.*, Phys. Lett. **B673** (2009) 127.
- [19] COMPASS Collaboration, F. Gautheron *et al.*, CERN-SPSC-2010-014, SPSC-P-340, 17 May 2010.
- [20] X.-D. Ji, Phys. Rev. Lett. **78** (1997) 610.
- [21] A. V. Belitsky *et al.*, Nucl. Phys. **B629** (2002) 323.
- [22] H1 Collaboration, F. D. Aaron *et al.*, Phys. Lett. **B659** (2008) 796.
- [23] Zeus Collaboration, S. Chekanov *et al.*, JHEP **05** (2009) 108.
- [24] Conceptual Design Report (CDR) for The Science and Experimental Equipment for The 12 GeV Upgrade of CEBAF (Prepared for the DOE Science Review, April 6–8, 2005), Editors J. Arrington *et al.*, Jefferson Lab (2005), http://www.jlab.org/div_dept/physics_division/GeV/doe_review/CDR_for_Science_Review.pdf.
- [25] M. Vanderhaeghen *et al.*, Phys. Rev. **D60** (1999) 094017.
- [26] K. Kumerički and D. Müller, Nucl. Phys. **B841** (2010) 1.
- [27] J. C. Collins, Phys. Lett. **B536** (2002) 43.
- [28] M. Anselmino *et al.*, in Proceedings of Transversity 2008: II International Workshop on Transverse Polarization Phenomena in Hard Scattering Processes, 27–31 May 2008, Ferrara, Italy; World Scientific, ed. by G. Ciullo *et al.*, April 2009, ISBN:978-981-4277-77-8, p. 138.